ACS Energy LETTERS

http://pubs.acs.org/journal/aelccp

FOCUS REVIEW

Design and Utilization of Infrared Light for Interfacial Solar Water Purification

Xiuqiang Li,* Thomas Cooper, Wanrong Xie, and Po-Chun Hsu*

Cite This: *ACS Energy Lett.* 2021, 6, 2645−2657

Read Online

ACCESS | Metrics & More | Article Recommendations

ABSTRACT: Clean drinking water is increasingly perceived as one of the most critical global challenges. Direct solar desalination with a minimal carbon footprint is a promising technology to alleviate the water challenge. However, this technology still faces a series of problems, such as poor salt-rejection of the absorber and low condensation efficiency and water output. Currently, the design and utilization of infrared light shows unique advantages in solving these problems. With this background, this Focus Review aims to summarize the state-of-the-art progress of three infrared-light-based strategies for direct solar desalination: the use of selective absorbers to obtain higher solar-to-vapor conversion efficiency, the use of radiative energy to indirectly heat the water to resolve the salt-rejecting problem of the absorber, and use of radiative cooling to enhance the output of freshwater. Also, unsolved scientific and technical issues associated with the outlook in these directions are discussed, with the hope of further promoting direct solar desalination for sustainability and global welfare.

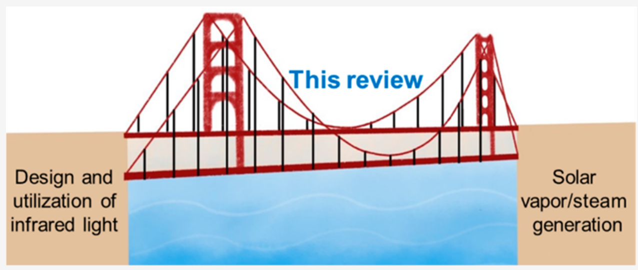

Water is an essential element of our human existence. Although we have abundant water resources on the earth, the lack of drinking water resources is a serious issue. About 29% of people in the world do not have access to safe drinking water, and 6% of deaths in underdeveloped countries are caused by drinking unsafe water.[1−3] Additionally, the shortage of drinking water resources will continue to increase. According to a report by the United Nations Development Programme 6, by 2050, it is predicted that this water shortage will worsen, and at least 1 in 4 people will suffer from the water crisis because of increasing drought and desertification.[4]

Direct solar desalination, which produces drinking water directly using solar energy with a minimal carbon footprint, is a promising technology to alleviate the water crisis. According to evaporation theory, liquid water tends to evaporate into the ambient until the vapor's partial pressure in air is equal to the saturation pressure of water at a given temperature. Because saturation pressure increases exponentially with temperature, when the water temperature at the evaporation interface is increased by solar heating, a significantly higher saturation pressure will occur.[5] In other words, more water needs to enter the ambient to achieve this balance, thus promoting evaporation. Meanwhile, the absorber temperature increase will generate corresponding heat conduction, heat convection, and heat radiation losses. A steady-state energy balance on the absorber can be described by the following equation:[6,7]

> Direct solar desalination, which produces drinking water directly using solar energy with a minimal carbon footprint, is a promising technology to alleviate the water crisis.

$$\dot{m}h_{\mathrm{fg}} = A\alpha q_{\mathrm{solar}} - A\varepsilon\sigma(T^4 - T^4_{\infty}) - Ah(T - T_{\infty}) - A\lambda \mathrm{d}T/\mathrm{d}x \quad (1)$$

where $\dot{m}$ is the mass flow rate of vapor, h_{fg} the latent heat, A the area of absorber, α the absorption coefficient, q_{solar} the solar irradiance, ε the emissivity of absorber, σ the Stefan−Boltzmann constant, T the temperature of absorber, T_{∞} the temperature of ambient, h the convection coefficient, and λ the thermal conductivity of absorber. However, traditional volumetric heating methods (blackening the bottom of the container or dispersing nanoparticles in bulk water to achieve

Received: April 26, 2021
Accepted: June 11, 2021
Published: July 1, 2021

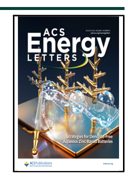

https://doi.org/10.1021/acsenergylett.1c00869
ACS Energy Lett. 2021, 6, 2645−2657

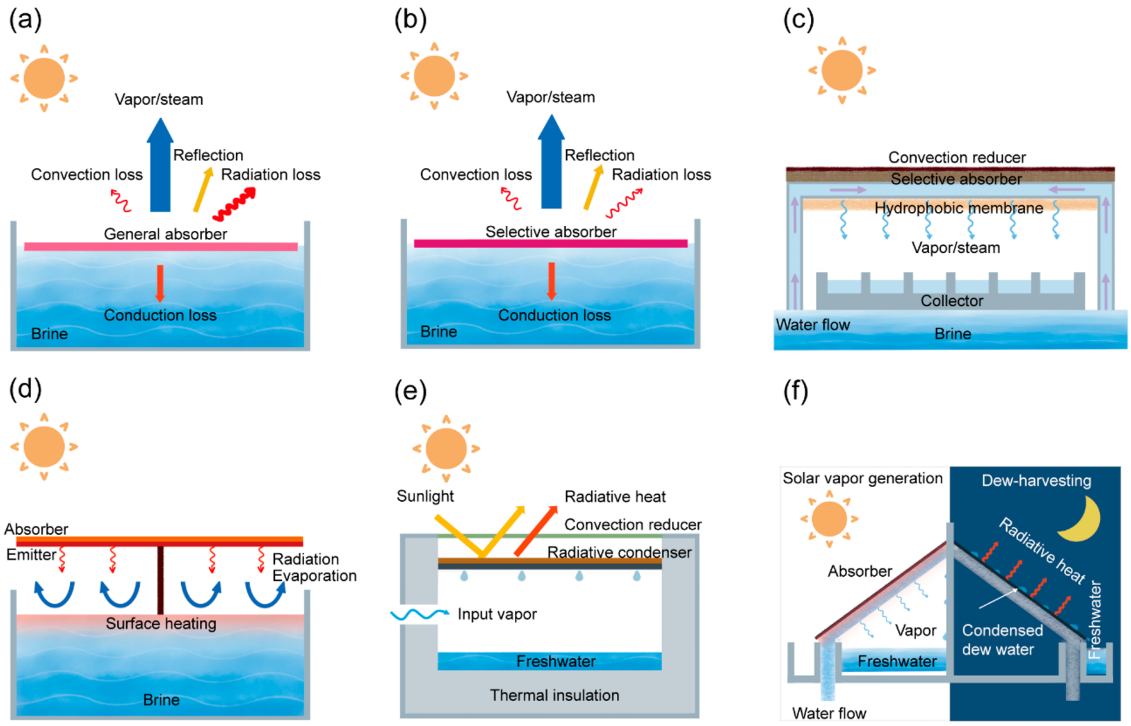

Figure 1. Schematics of (a) interfacial solar vapor generation; (b) interfacial solar vapor generation with a permeable selective absorber (radiation loss is suppressed); (c) interfacial solar vapor generation with a nonpermeable selective absorber (the water vapor does not pass through the absorber but usually evaporates and condenses under the absorber); (d) contactless solar vapor/steam generation via downward thermal radiation; (e) daytime radiative condenser; (f) all-day freshwater harvesting through combining solar vapor generation and dew-harvesting.

heating) is inefficient (∼40%).[6] The concept of interfacial solar vapor/steam generation was recently proposed to improve heat localization at the liquid surface to make this technology more efficient (Figure 1a). In the past few years, this field has developed rapidly and has made significant progress toward maximizing performance and water output.[8−27] For example, the solar-to-vapor/steam conversion efficiency can reach >90% under one sun (1000 W/m^2) illumination through material design and photon and heat management. Readers are directed to the many comprehensive reviews that summarize this aspect of the research.[28−40] However, poor salt rejection of the absorber and low condensation efficiency and and water output, among other practical challenges, still hinder this technology's widespread adoption.

In the past decade, significant progress has been achieved by design and utilization of infrared light, such as (1) use of permeable (Figure 1b) or nonpermeable (Figure 1c) selective absorbers to suppress radiation losses for higher solar-to-vapor conversion efficiency, (2) use of radiative energy to indirectly heat the water (Figure 1d) to resolve the salt-rejecting problem of the absorber, and (3) use of radiative cooling (Figure 1e,f) to enhance the output of freshwater. These provide new opportunities to solve the problems mentioned above. Thus, this Focus Review aims to introduce the working principle, state-of-the-art progress, challenges, and perspectives of the above three directions, aiming to further promote the development of infrared spectrum-based technologies for solar desalination.

Use of Selective Absorbers to Obtain Higher Solar-to-Vapor Conversion Efficiency. In the solar−thermal conversion process, a selective absorber is a means to increase the working temperature and efficiency, in which the performance is determined by solar absorptivity (eq 2) and thermal emissivity (eq 3) (the ideal selective absorber absorption curve can be seen in Figure 2a). To date, a variety of high-performance selective absorbers have been developed and successfully applied to solar heating, solar power generation, catalysis, deicing, etc.[41−47]

$$\bar{\alpha} = \frac{\int_0^\infty d\lambda\ \alpha(\lambda)\ E_{\lambda,\mathrm{Solar}}(\lambda)}{q_{\mathrm{Solar}}} \tag{2}$$

$$\bar{\varepsilon} = \frac{\int_0^\infty d\lambda\ \varepsilon(\lambda)\ E_{\lambda,\mathrm{B}}(\lambda,\ T_\mathrm{A})}{\sigma T_\mathrm{A}{}^4} \tag{3}$$

where $\bar{\alpha}$ and $\bar{\varepsilon}$ are the total (spectrally integrated) solar absorptivity and thermal emissivity of the solar absorber; $\alpha(\lambda)$ and $\varepsilon(\lambda)$ are the spectral absorptivity and emissivity at wavelength λ, respectively; $E_{\lambda,\mathrm{Solar}}(\lambda)$ and $E_{\lambda,\mathrm{B}}(\lambda,\ T_\mathrm{A})$ are the solar spectral irradiance and blackbody spectral emissive power, respectively; q_{Solar} is the total solar irradiance (AM 1.5G, 1 kW m^{-2}); σ is the Stefan−Boltzmann constant, and T_A is the temperature of the absorber. Like other solar−thermal conversion technologies, the solar vapor/steam generation process is accompanied with radiation heat losses. Figure 2b shows the radiative heat losses of a blackbody absorber and a commercial selective absorber with 95% $\bar{\alpha}$ and 5% $\bar{\varepsilon}$ (assuming ambient temperature is 25 °C).[48] For solar vapor generation, the absorber temperature is typically 35−45 °C under one sun. In this case, the blackbody absorber will produce approximately 63−133 W/m^2 radiative heat loss, corresponding to the theoretical maximum solar-to-vapor conversion efficiency of 93.7% and 86.7% under one sun. Also, as the temperature

https://doi.org/10.1021/acsenergylett.1c00869
ACS Energy Lett. 2021, 6, 2645−2657

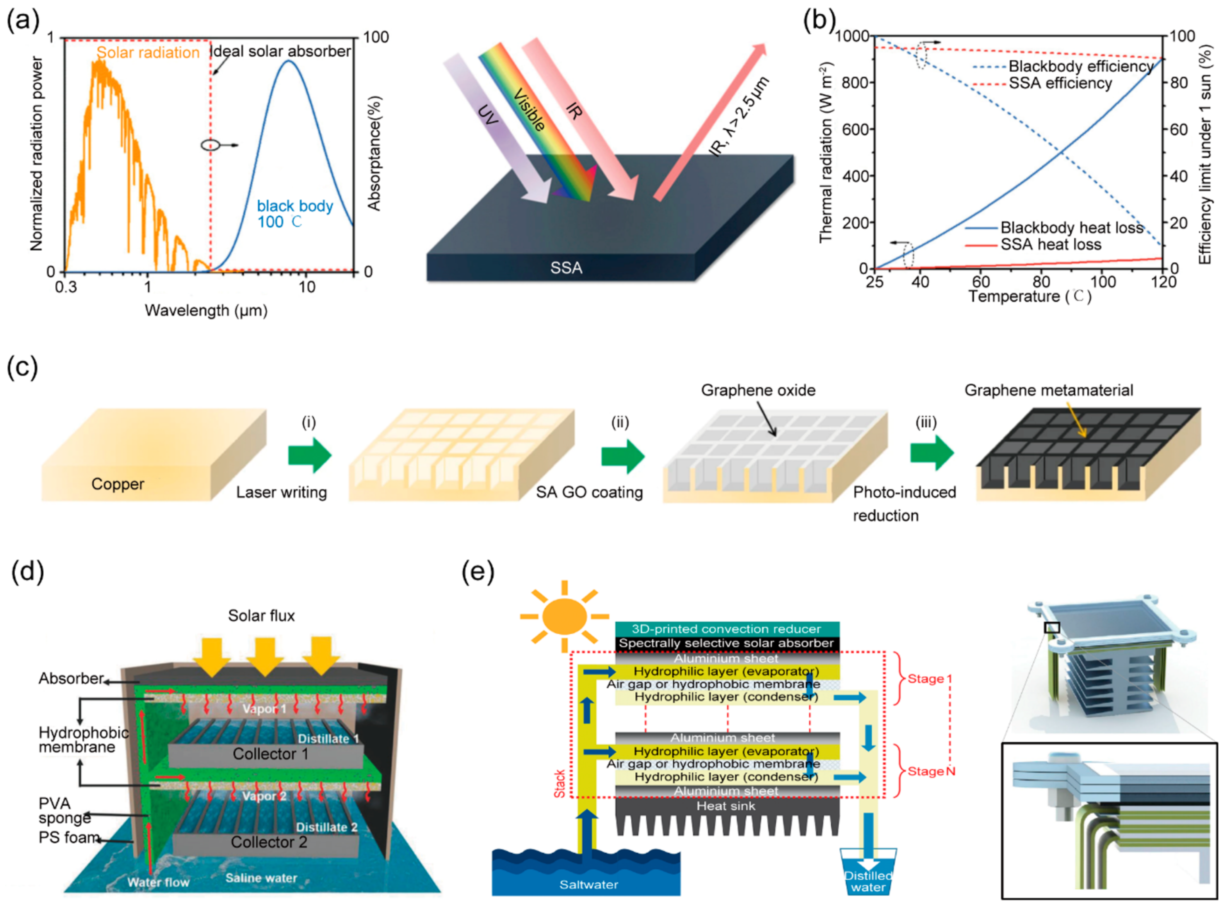

Figure 2. Selective absorbers for solar vapor generation. (a) AM 1.5G solar spectrum, 100 °C blackbody radiation spectrum, and the ideal selective absorber spectrum with a cutoff wavelength at 2.5 μm (left); schematic of the selective absorber (right). Reprinted with permission from ref 48. Copyright 2020 Wiley-VCH Verlag GmbH & Co. (b) Radiative heat loss and solar−thermal conversion efficiency limit of a blackbody absorber and a commercial selective absorber (SSA) with 95% $\bar{\alpha}$ and 5% $\bar{\varepsilon}$ over temperature under one sun. Reprinted with permission from ref 48. Copyright 2020 Wiley-VCH Verlag GmbH & Co. (c) Schematic of the preparation process of three-dimensional structured graphene metamaterial. Reprinted with permission from ref 51. Copyright 2020 Nature Publishing Group. (d) Schematic of the solar vapor generation device with a two-level collector. Reprinted with permission from ref 56. Copyright 2018 Wiley-VCH Verlag GmbH & Co. (e) Schematic (left) and setup (right) of the solar vapor generation device with a ten-level collector. Reprinted with permission from ref 57. Copyright 2018 Nature Publishing Group.

Table 1. Summary of Selective Absorber-Based Solar Vapor Generation Contributions

permeability	materials and optical properties	performance	reference
permeable	commercially cermet-based selective absorber with 93% $\bar{\alpha}$ and 7% $\bar{\varepsilon}$	100 °C steam under one sun	7
permeable	C-Au-TiO_2	63.7% solar-to-vapor conversion efficiency under one sun	49
permeable	nickel on anodized aluminum oxide (AAO) (with > 80% $\bar{\alpha}$ and ∼ 20% $\bar{\varepsilon}$)	73% solar-to-vapor conversion efficiency under one sun	50
permeable	graphene metamaterial with > 80% $\bar{\alpha}$ and < 5% $\bar{\varepsilon}$	>90% solar-to-vapor conversion efficiency under one sun	51
permeable	commercially selective solar absorber (Alanod) with 99% $\bar{\alpha}$	2.42 kg m^{-2} h^{-1} water evaporation rate under one sun	52
permeable	Au/AAO (Alanod) (>90% $\bar{\alpha}$)	65% solar-to-vapor conversion efficiency under 4 sun	53
nonpermeable	solar vacuum tube (Shanghai Hanyan Industrial Co., Ltd.) with 93% $\bar{\alpha}$ and 7% $\bar{\varepsilon}$	121 °C steam under 600 W/m^2	54
nonpermeable	$TiNO_x$ with 95% $\bar{\alpha}$ and 5% $\bar{\varepsilon}$	48% solar-to-vapor conversion efficiency under one sun	55
nonpermeable	commercial spectrally selective absorber (Bluetec, Germen) with 95% $\bar{\alpha}$ and 5% $\bar{\varepsilon}$	72% solar-to-vapor conversion efficiency under one sun	56
nonpermeable	$TiNO_x$ with 95% $\bar{\alpha}$ and 4% $\bar{\varepsilon}$	3 L/m^2 h output from seawater in a 10-stage configuration	57
nonpermeable	selective absorber with >90% $\bar{\alpha}$ and <10% $\bar{\varepsilon}$	128 °C steam under one sun	58

increases, the radiative heat loss increases significantly. When the absorber temperature reaches 100 °C, the blackbody absorber produces ∼650 W/m^2 radiative loss, bringing the maximum efficiency down to 35%. In contrast, a selective absorber with $\overline{\alpha}$ = 0.95 and $\overline{\varepsilon}$ = 0.05 could still theoretically achieve a conversion efficiency of 91.8% even at 100 °C temperature, making selective absorbers the better choices for solar vapor/steam generation. To date, the use of selective absorbers can be divided into two categories: nonpermeable and permeable (see Table 1), as elaborated in the following paragraphs.

This Focus Review aims to summarize the state-of-the-art progress of three infrared-light-based strategies for direct solar desalination: the use of selective absorbers to obtain higher solar-to-vapor conversion efficiency, the use of radiative energy to indirectly heat the water to resolve the salt-rejection problem of the absorber, and use of radiative cooling to enhance the output of freshwater.

Use of Permeable Selective Absorbers. The porous structure of permeable selective absorber ensures upward escape channels for vapor/steam. Moreover, it can effectively suppress the absorber's radiation heat loss.[7,49−53] Wang et al.[50] prepared permeable selective absorbers (with >80% $\overline{\alpha}$ and ∼20% $\overline{\varepsilon}$) by depositing nickel on anodized aluminum oxide (AAO) by a pulsed electrodeposition (PED) method to maximize the absorption of sunlight and minimize the radiative loss of the absorber. As a result, 73% of overall efficiency can be achieved under one sun. Also, a 10% enhancement in water evaporation rate is found by using the prepared Ni/AAO selective absorber compared to a graphite absorber. Lin et al.[51] demonstrated a permeable selective absorber, three-dimensional structured graphene metamaterial (SGM), which achieves high absorbance (>80%) over broadband wavelengths from ultraviolet to near-infrared radiation (IR) regime and low emission rate (<5%) in the IR regime. As shown in Figure 2c, the preparation process is mainly divided into three steps: (1) The trench-like structures were fabricated on the copper substrate using direct laser printing. (2) After patterning, a 40 nm thick graphene oxide (GO) metamaterial film was deposited by a water-based self-assembly process. The GO film coating was designed to generate three-dimensional (3D) GO cavities through the trenches' sidewalls. (3) The ∼30 nm graphene metamaterial was obtained by photoreduction of GO-coating. The result showed that >90% solar-to-vapor conversion efficiency was achieved by using SGM. Permeable selective absorbers have also been used to increase the vapor temperature. For example, Ni et al.[7] used a commercially cermet-based selective absorber (with 93% $\overline{\alpha}$ and 7% $\overline{\varepsilon}$) with thermal concentration by conducting the absorbed heat into the evaporation area for solar vapor generation. By combining transparent insulating bubble wrap to suppress convection loss and thermally insulating floating foam to suppress conduction loss, the result showed that 100 °C steam was achieved under one sun.

Use of Nonpermeable Selective Absorbers. Unlike permeable absorbers that allow vapor to directly escape to the environment, nonporous selective absorbers do not provide pathways for the vapor to travel upward to the environment. Therefore, a more complex architecture, where evaporation and condensation occur within a chamber below the absorber, is typically adopted.[54−58] Chang et al.[55] used nonpermeable selective absorbers (commercial $TiNO_x$ with 95% $\overline{\alpha}$ and 5% $\overline{\varepsilon}$) to enhance the optical absorption and suppress thermal radiation. Meanwhile, a layer of quartz glass was placed on the absorber to suppress conduction and convection losses. As a result, ∼48% solar-to-vapor conversion efficiency was successfully achieved under one sun. To increase water production, multistage structures are also developed to recycle the latent heat of vapor condensation. Xue et al.[56] used selective absorbers with 95% $\overline{\alpha}$ and 5% $\overline{\varepsilon}$ as solar absorbers and designed a two-stage solar desalination device to recycle the water vapor's latent heat (Figure 2d). The result showed that a 1.02 kg/m^2 h evaporation rate and 72% solar-to-vapor conversion efficiency under one sun could be achieved with a two-level collector device. Chiavazzo et al.[57] also used commercial selective absorbers ($TiNO_x$, with 95% $\overline{\alpha}$ and 4% $\overline{\varepsilon}$) to increase the solar radiation's conversion efficiency into heat. In the device (Figure 2e), each unit stage comprises two hydrophilic layers separated by a hydrophobic microporous membrane without extra mechanical support. The result showed that 3 L/m^2 h output from seawater in a 10-stage configuration was achieved under laboratory conditions, twice the yield of current passive complete distillation systems (theoretical modeling shows a potential up to 6 L/m^{2}h). In addition to increasing water production, nonpermeable selective absorbers are also used to increase vapor temperature. Zhao et al.[58] achieved 128 °C steam using a nonpermeable selective absorber with >90% $\overline{\alpha}$ and <10% $\overline{\varepsilon}$ combining optical concentration with other thermal management technologies.

Use of Radiative Energy to Indirectly Heat the Water to Resolve the Salt-Rejecting Problem of the Absorber. As mentioned above, interfacial solar heating can significantly improve the conversion efficiency of solar-to-vapor/steam. On the other hand, it also brings a vital salt accumulation issue in the solar absorber which consequently reduces the evaporative performance because of the reduced optical absorption, clogged water supply channel, and/or damaged structure of the absorber, etc., especially for high-concentration brine.[59,60] For example, Xu et al.[61] demonstrated that the performance of a traditional floating solar absorber (carbon black nanoparticles coating polyacrylonitrile) decreased by ∼15% after 16 days of operation. A device that can address this issue is crucial to the development of direct solar desalination.

To date, several strategies have been proposed and proven to be effective in reducing salt accumulation (see Table 2). These include (1) optimizing the water supply channel to increase the ion diffusion between the solar absorber and the bulk water:[62−68] Kuang et al.[62] reported a natural wood with millimeter-sized drilled channels and micron-sized natural wood channels, which can quickly exchange the salt with the bulk solution, enabling the real-time self-cleaning of the absorber. The result showed 75% solar-to-vapor conversion efficiency in a highly concentrated salt solution (20 wt % NaCl) can be achieved under one sun irradiation, as well as long-term stability (over 100 h of continuous operation). Zhang et al.[67] designed a fluidic structure with three key parts, which include a water-wicking inlet, a hydrophilic solar absorber, and a wicking outlet. In this system, salt can be promptly swept away into the brine discharge by the running fluid to avoid salt accumulation on the absorber. The result

https://doi.org/10.1021/acsenergylett.1c00869
ACS Energy Lett. 2021, 6, 2645−2657

Table 2. Summary of Salt Rejection Experimental Work

salt rejection strategies	contact method	performance	reference
optimizing the water supply	contact	75% solar-to-vapor conversion efficiency in a highly concentrated salt solution (20 wt % NaCl) under one sun; over 100 h of continuous operation without salt precipitation	62
optimizing the water supply	contact	52 ± 2.5% solar-to-vapor conversion efficiency at 600 W/m^2; 30 h under one sun without detectable salt crystal formation	63
optimizing the water supply	contact	93.3% solar-to-vapor conversion efficiency under one sun; 12 h under one sun without salt fouling	64
optimizing the water supply	contact	1.47 kg m^{-2} h^{-1} evaporation rate under one sun; 12 h under one sun without salt precipitation	65
optimizing the water supply	contact	enabling 100 h continuous solar desalination under 1 sun with greater than 80% evaporation efficiency	66
optimizing the water supply	contact	stable solar-to-vapor conversion efficiency (92%) in 10 wt % NaCl salt solution under one sun in 100 h and 30 days continuous desalination tests	67
optimizing the water supply	contact	~1.63 kg m^{-2} h^{-1} evaporation rate under one sun; after 50 continuous cycles of water extraction without detectable salt crystal formation	68
using hydrophobic solar absorber	contact	~80% solar-to-vapor conversion efficiency out of high-salinity brine (10 wt %) and wastewater containing heavy metal ions (30 wt %); showing an average evaporation rate of 1.27 kg m^{-2} $hour^{-1}$ over 18 days	69
using hydrophobic solar absorber	contact	~86.9% solar-to-vapor conversion efficiency under one sun; stable evaporation rate over 400 min of continuous operation or 90 d of intermittent work	70
using hydrophobic solar absorber	contact	~86.6% solar-to-vapor conversion efficiency under one sun; over 15 days of continuous desalination without decay	71
adjusting the hydrophobicity or evaporation site of the solar absorber	contact	showing an average evaporation rate of 2.42 kg m^{-2} h^{-1} over 288 h of continuous operation	52
adjusting the hydrophobicity or evaporation site of the solar absorber	contact	89.9% solar-to-vapor conversion efficiency under one sun; after 12 h evaporation without salt accumulation	72
adjusting the hydrophobicity or evaporation site of the solar absorber	contact	a clean water productivity of >3 kg m^{-2} per day; without noticeable water evaporation rate decay in at least 120 h out of 25 wt % salt concentration	73
adjusting the hydrophobicity or evaporation site of the solar absorber	contact	>96% solar-to-vapor conversion efficiency under one sun out of high salinity (25 wt % NaCl); stable evaporation rate to the seawater for 10 days under one sun illumination for 9 h every day	74
adjusting the hydrophobicity or evaporation site of the solar absorber	contact	81.2% solar-to-vapor conversion efficiency under one sun; achieving continuous vapor generation and salt harvesting in over 600 h of nonstop operation	75
tuning the size of water supply channel of the solar absorber	contact	79% solar-to-vapor conversion efficiency under one sun; without salt accumulation after 5 days evaporation	76
tuning the charge of the solar absorber	contact	~1.3 L per m^2 per hour evaporation rate under 1 sun; after 72 h consecutive evaporation without salt accumulation on absorber	77
absorber's downward thermal radiation heating	contactless	133 °C steam	78
absorber's downward thermal radiation heating	contactless	43% solar-to-vapor conversion efficiency under one sun	79
absorber's downward thermal radiation heating	contactless	1.94 kg m^{-2} h^{-1} evaporation rate under 2.6 sun	80

https://doi.org/10.1021/acsenergylett.1c00869
ACS Energy Lett. 2021, 6, 2645−2657

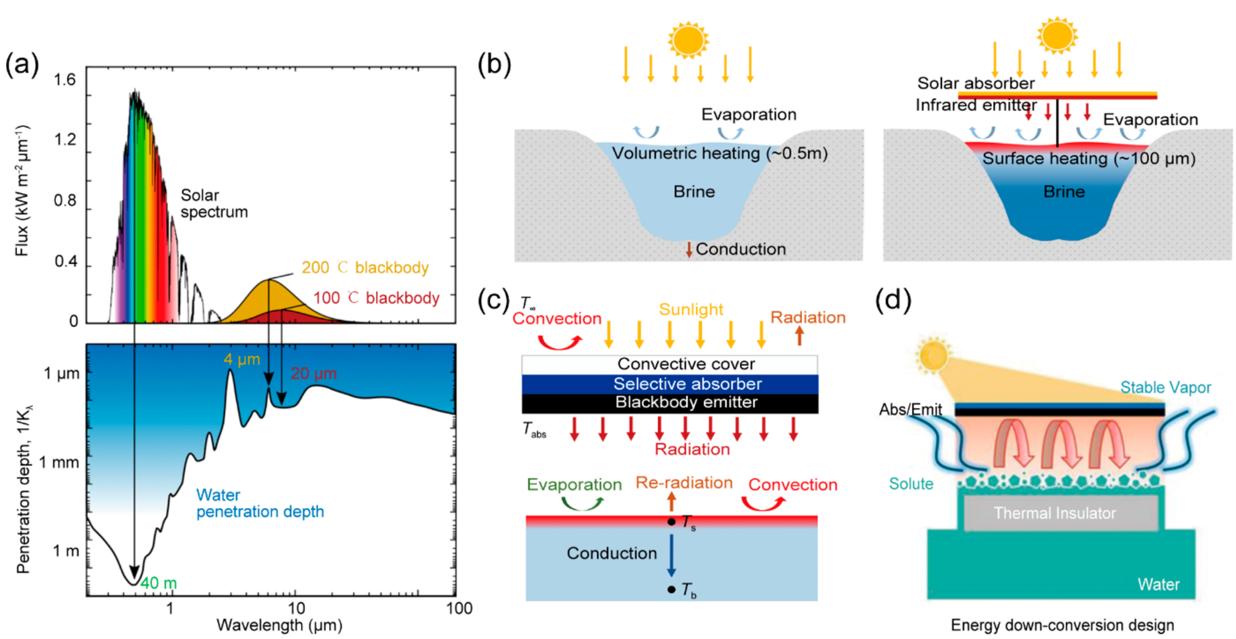

Figure 3. Solar vapor/steam generation via downward thermal radiation. (a) Top panel: solar spectrum and thermal blackbody sources at 100 and 200 °C. Bottom panel: photon penetration depth for liquid water. Reprinted with permission from ref 78. Copyright 2018 Nature Publishing Group. (b) Schematic of a conventional evaporation pond (left) and solar umbrella (a spectrally selective absorber and blackbody emitter) for contactless water purification. Reprinted with permission from ref 79. Copyright 2020 Nature Publishing Group. (c) Energy balance for the umbrella and water. Reprinted with permission from ref 79. Copyright 2020 Nature Publishing Group. (d) Working principle of the contactless solar evaporator with thermal insulation at water surface during solute accumulation. Reprinted with permission from ref 80. Copyright 2021 Wiley-VCH Verlag GmbH & Co.

showed that stable 92% solar-to-vapor conversion efficiency in a highly concentrated salt solution (10 wt % NaCl) under one sun in long-cycle continuous desalination tests (100 h and 30 days) can be achieved. (2) Using a hydrophobic solar absorber:[69−71] Xu et al.[69] reported a water lily-inspired hierarchical structure with excellent hydrophobic properties that enables ~80% solar-to-vapor efficiency out of high-salinity brine (10 wt %) and wastewater containing heavy metal ions (30 wt %) and shows an average evaporation rate of 1.27 kg m^{-2} $hour^{-1}$ over 18 days of continuous operation. (3) Adjusting the hydrophobicity or evaporation site of the solar absorber to allow the salt to precipitate in a specific area:[52,72−75] Shi et al.[73] designed a 3D cup-shaped solar evaporator, which can separate the light-absorbing surface from the salt precipitation surface to avoid the 3D solar evaporator affected by the salt crust layer. As a result, it can be operated at a high salt concentration of 25 wt % without a significant water evaporation rate decrease of over 120 h. Wu et al.[74] designed a biomimetic triangular pyramid, which can achieve localized salt crystallization at the apex of the triangular pyramid. This biomimetic 3D structure showed >96% solar-to-vapor conversion efficiency under one sun out of high salinity (25 wt % NaCl) and stable evaporation rate to the seawater for 10 days under one sun illumination for 9 h every day. (4) Tuning the charge of the solar absorber or the size of the water supply channel to block ions from entering the absorber, etc.:[76,77] Zeng et al.[77] demonstrated a new liquid-pumping mechanism using a poly electrolyte hydrogel with high osmotic pressure for liquid pumping and high ionic strength for salt rejection. The result showed a ~1.3 L/m^2 h evaporation rate under one sun was achieved. Also, no salt precipitation was seen on the surface of the absorber after 72 h of continuous operation. However, these will reduce the conversion efficiency or increase the need for extra removal processes. Therefore, salt accumulation is still a challenge for interfacial heating that needs further investigation.

To further solve the salt-rejecting problem of the solar absorber, Cooper et al.[78] first proposed contactless solar vapor/steam generation via the absorber's downward thermal radiation. This technology avoids direct contact between the absorber and bulk water and aims to completely solve the absorber's salt-rejecting problem. Water evaporation is an endothermic process. Therefore, a necessary step for solar-powered water evaporation is delivering the energy from solar photons to the water. The basis for the implementation of the noncontact approach is that water molecules have strong absorption of infrared light. According to the Beer−Lambert law[78]

$$\tau_\lambda(L) = I_\lambda(L)/I_{\lambda,0} = e^{-\kappa_\lambda L} \quad (4)$$

where $\tau_\lambda(L)$ is the spectral transmittance (1 − absorptance), I_λ the intensity of a beam at a distance L, $I_{\lambda 0}$ the incident intensity at $L = 0$, and $1/\kappa_\lambda$ the mean penetration depth in water of a photon of wavelength λ. The calculated penetration depth (Figure 3a) indicates water is a poor absorber at visible and near-infrared wavelengths (the depth required to absorb 90% of the solar energy is larger than 20 m). On the other hand, mid-infrared wavelengths are strongly absorbed by water (most within a 100 μm layer). For example, superimposed in Figure 3a are the blackbody radiation bands of 100 and 200 °C, which peak at 20 and 4 μm, respectively. When operating in these wavelength regimes, the absorbed solar heat can be localized within a very narrow layer at the evaporation surface. Because of the shifting of solar radiation to mid-infrared and larger wavelengths combined with localized heating at the evaporation surface, a higher evaporation rate can be achieved.

https://doi.org/10.1021/acsenergylett.1c00869
ACS Energy Lett. 2021, 6, 2645−2657

After the concept of contactless solar vapor/steam generation was put forward by Cooper et al. and showed a promising application in seawater desalination, Menon et al.[79] gave a detailed analysis and extended this technology to the field of wastewater treatment. This process can be divided into three steps: the processes of absorption, emission, and heating; therefore, the overall system efficiency (η) can be expressed as

$$\eta = \dot{m}h_{fg}/q_{solar} = \eta_1 \times \eta_2 \times \eta_3 \tag{5}$$

$$\eta_1 = (\alpha_s q_{solar} - \varepsilon_s \sigma T_{abs}^4) \tag{6}$$

$$\eta_2 = F\varepsilon_b \sigma T_{abs}^4/(\alpha_s q_{solar} - \varepsilon_s \sigma T_{abs}^4) \tag{7}$$

$$\eta_3 = \dot{m}h_{fg}/F\varepsilon_b \sigma T_{abs}^4 \tag{8}$$

where $\dot{m}$ is mass flow rate of vapor, h_{fg} the latent heat, q_{solar} the solar intensity, η_1 the absorber optical efficiency, η_2 the emitter efficiency, η_3 the evaporation efficiency, α_s the solar absorption of absorber, ε_s the emissivity of the upper surface of the absorber, σ the Stefan–Boltzmann constant, T_{abs} the temperature of absorber, F the radiation view factor, and ε_b the emissivity of the lower surface of the absorber/emitter. To obtain a high η_1 (eq 4), that is to suppress the optical losses to improve the conversion efficiency of sunlight into heat, the efficient selective absorber is the ideal choice because it can simultaneously absorb solar energy (200–2500 nm, high α_s) and suppress infrared radiation (>2.5 μm, low ε_s). To obtain a high η_2 (eq 5), it is necessary to increase the ε_b and F. On the other hand, the heat losses, including conduction and convection of absorber/absorber+emitter also should be suppressed to improve the T_{abs}. Finally, to obtain a high η_3 (eq 6), thermal losses, including conduction, convection, and radiation from the water surface, should be minimized to maximize the useful energy to promote water evaporation. Moreover, they reported a photothermal umbrella for wastewater treatment (as shown in Figure 3b,c), which consists of three layers: convex layer (bubble wrap), selective absorber (TiNOX Energy on aluminum with 0.95 of solar absorptance and 0.04 emittance at thermal wavelengths), and blackbody emitter (Zynolyte Hi-Temp Paint with 0.94 emittance at thermal wavelengths; Aervoe). As discussed in the previous paragraph, choosing a selective absorber can increase η_1. The selection of the convective layer and the blackbody emitter can efficiently improve η_2. At the same time, benefiting from heat localization at the water's surface through the radiative coupling, the results show that an overall solar–thermal conversion efficiency of 43% (evaporation rate of 0.62 kg/m^2 h, η_1 = 91%, η_2 = 74%, and η_3 = 63%) under one sun can be achieved, which is equal to enhancement in evaporation of >100% compared with volumetric heating (as shown in Figure 3b). Currently, Bian et al.[80] further applied a 2D water channel with thermal insulation to reduce the heat conduction from the heating water surface to bulk water to increase η_3 for wastewater treatment (Figure 3d). The result showed that the designed evaporator enables a high evaporation rate of 1.94 kg/m^2 h under 2.6 sun illumination during a continuous solute accumulation process for 32 h.

A unique, and only partially explored, advantage of radiative heating is the ability to control the heat flux through radiative shielding. Equation 7 shows that the emitter efficiency increases as the view factor between the water and emitter is increased. However, this increase in efficiency comes with a concomitant decrease in absorber/emitter temperature. In other words, decreasing the view factor has the effect of increasing the thermal resistance between the emitter and water, which causes a larger temperature difference to develop between the water and emitter for the same heat flow rate. The view factor can be effectively modified by placing a reflective shield between the emitter and water surfaces. While decreasing absorber/emitter temperature is usually desirable from the perspective of reducing heat losses, there may be situations where it is desirable for it to increase. For example, Cooper et al.[78] showed that by passing the generated vapor through the porous absorber, it can be superheated to temperatures of 122 °C under one sun illumination. By placing a reflective radiation shield with the small hole between the emitter and water surface, it was shown that the steam temperature can be boosted to 133 °C. What is perhaps of even more interest, and has yet to be explored, is the ability to actively control the absorber/emitter temperature (and thus vapor outlet temperature) by changing the size of the hole in the radiation shield. This could be achieved, for example, by utilizing an iris diaphragm or similarly adjustable radiation shield between the emitter and water. Under real outdoor conditions, the incident solar irradiance is intermittent, causing fluctuations in absorber/emitter and steam temperature. Control of the emitter-to-water view factor via the adjustable shield would allow the temperature to be maintained at a constant level even during fluctuations in the incident solar irradiance. This may prove important in a number of different situations, for example, (1) when a minimum steam outlet temperature is required, (2) when a minimum structure temperature is desired to suppress biofouling, and (3) when fluctuations in temperature would lead to significant thermally induced shocks and stresses in the structure. The ability to control temperature through variable shielding seems to be a unique feature of contactless radiative heating, which could not easily be replicated in conventional contact (conduction) heating approaches.

Use of Radiative Cooling to Enhance the Output of Freshwater. During direct solar desalination, apart from the evaporation step mentioned above, the other necessary step is to condense the vapor/steam by dissipating the heat of condensation into the surrounding environment, mainly by convection and conduction. Benefitting from the interfacial solar heating, the evaporation efficiency of recent devices has been greatly improved, resulting in evaporation efficiencies approaching the theoretical limit assuming all the absorbed solar energy can be utilized for evaporation. However, the condensation efficiency from convection and conduction usually is much lower than the evaporation efficiency, with the final water output ultimately limited by the condensation step.[81−83] For example, the evaporation rate of interface heating usually may reach 1.4 kg/m^2 h under one sun, but the final freshwater output is only about 2–4 L/day.[64] Using radiative dew condensation without energy input is a promising strategy to enhance condensation efficiency. However, traditional radiative dew condensers are incompatible with direct solar desalination devices because they achieve subambient cooling only at night because absorbed solar energy during the day would otherwise overwhelm the radiative cooling power.[84,85] Recently, Raman et al.[86] demonstrated daytime radiative cooling by integrating a high-efficiency solar reflector to reflect solar energy with a high mid-IR emissivity emitter to radiate the energy (8–13

https://doi.org/10.1021/acsenergylett.1c00869
ACS Energy Lett. 2021, 6, 2645–2657

Table 3. Summary of Contributions Related to Radiative Cooling for Enhancing the Output of Freshwater

experimental method	materials	performance	reference
experimental	polydimethylsiloxane (PDMS) and silver (Ag) on an aluminum (Al) substrate, with thickness of 100 μm, 150 nm, and 1 mm	twice higher than commercial condenser	97
experimental	PDMS/multiwalled carbon nanotubes onto polycarbonate substrate	71.1% solar-to-vapor conversion efficiency under one sun and 0.1 L m^{-2} day^{-1} dew water collection rate at night	99
theoretical		At $T_{ambient}$ = 20 °C with RH = 40%, the selective emitter achieves 13 g/m^2 hr of mass flux.	100

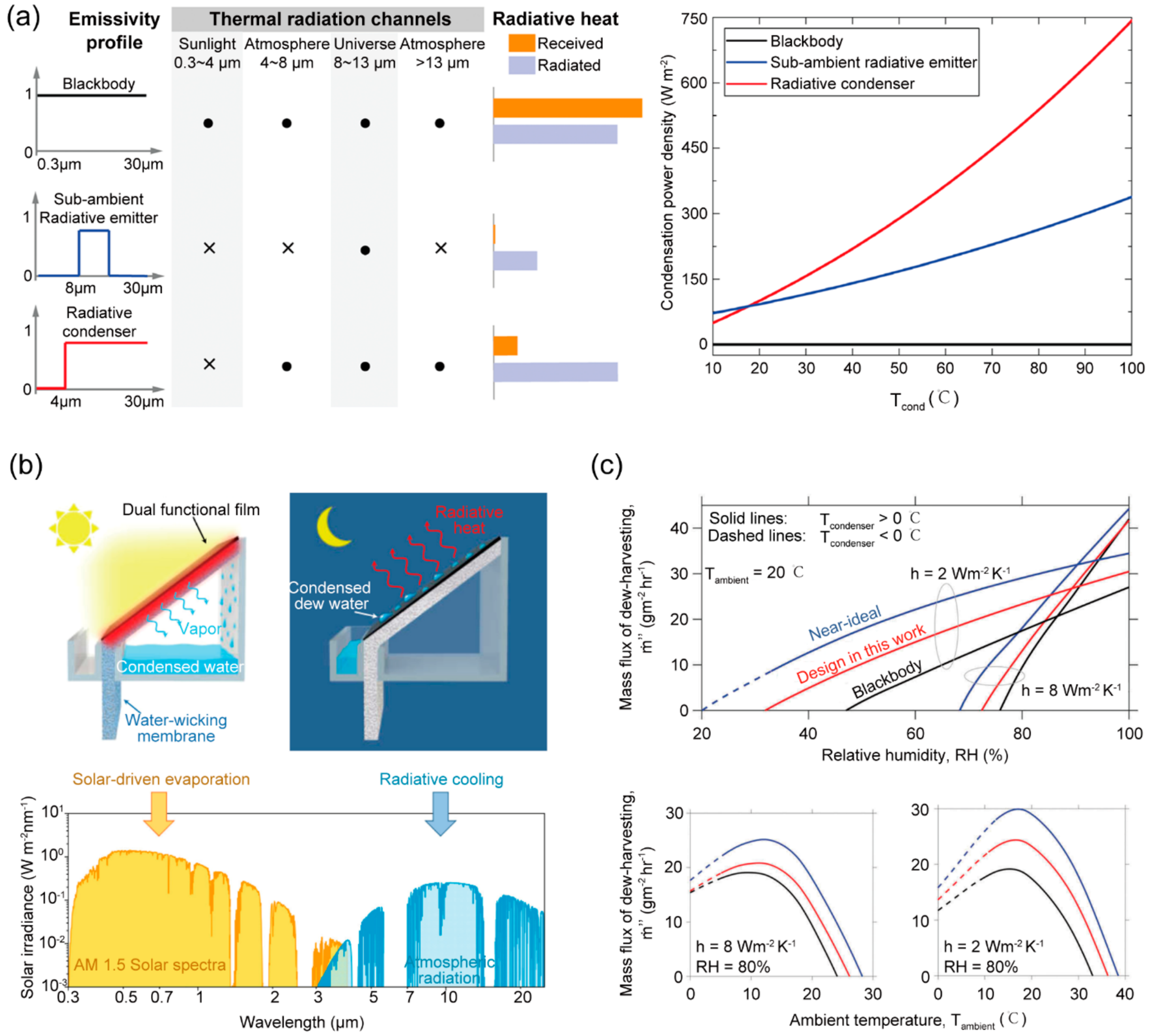

Figure 4. Radiative cooling for solar vapor generation. (a) Emissivity properties (left) and calculated condensation power (right) of a blackbody (black), the subambient radiative emitter (blue), and radiative condenser (red). Reprinted with permission from ref 97. Copyright 2021 National Academy of Sciences. (b) Schematic illustrating of work principle of all-day freshwater harvesting through combing solar vapor generation and dew-harvesting. Reprinted with permission from ref 99. Copyright 2020 American Chemical Society. (c) Mass flux of dew-harvesting at different boundary conditions. Reprinted with permission from ref 100. Copyright 2020 Taylor & Francis.

μm) to deep space through the atmospheric window. To date, a series of efficient daytime radiative cooling materials with good performance (usually between 60 and 150 W/m^2) have been developed.[87−96] Compared with traditional radiative dew condensers that function during the nighttime, daytime radiative cooling technology provides a new opportunity to integrate daytime radiative dew condensation and direct solar desalination devices (see Table 3).

Recently, Zhou et al.[97] carried out theoretical and experimental research on the integration of daytime radiative dew condensation and direct solar desalination devices and analyzed the influence of different spectra (blackbody, subambient radiative emitter, and radiative condenser, as shown in Figure 4a left) on condensation performance. The condensation power density can be expressed as

$$q_{cond} = \int d\Omega \cos\theta \int_0^\infty d\lambda (I_{BB}(T_{cond}, \lambda) - I_{atm}(T_{cond}, \lambda) - I_{AM1.5}(\lambda)\varepsilon_{cond}(\lambda, \theta) \tag{9}$$

where ε_{cond} (λ, θ) is the angle-dependent emissivity of the condenser, I_{BB} (T, λ) the spectral intensity of a blackbody at temperature T, $I_{AM1.5}$ the standard solar spectral intensity, and $I_{atm}(T_{amb}, \lambda)$ the spectral intensity of the atmosphere at ambient temperature (assume T_{amb} = 20 °C). After calculation by eq 9, as shown in Figure 4a right, it can be seen that the condensation power density of radiative condensers (red line) is more than two times as large as subambient radiative emitters (blue line) at most vapor temperatures because the subambient radiative cooler can only reject heat to outer space, while the above-ambient radiative condenser can also reject heat to the atmosphere because of the condensers' elevated temperature. When the condensation temperature is 50 °C (which usually can be achieved under one sun), the radiative condensers' condensation power contributed by radiation can reach ~300 W. For direct solar desalination systems, the vapor temperature is usually higher than the ambient temperature. Therefore, compared with the subambient radiative emitter, the radiative condenser is more suitable for direct solar desalination systems.[98] In addition to the above theoretical analysis, Zhou et al.[97] also designed a PDMS/Ag material system with 96% solar reflectance (0.3−4 μm) and efficient mid-infrared emissivity (>4 μm). The outdoor test results showed that the daytime radiative condenser's water output is more than two times higher than that of the traditional commercial condenser.

In addition to enhancing condensation for direct solar desalination, the radiative cooling technology can also be combined with direct solar desalination for all-day freshwater harvesting. Specifically, the device can absorb solar energy to evaporate water for desalination in the daytime and passively cool down itself through radiative cooling to collect dew water at night. Xu et al.[99] demonstrated a dual-mode film (multiwalled carbon nanotube network bound by polydimethylsiloxane on the polycarbonate substrate) with ~95% solar absorption and ~90% emittance in the wavelength range of 8−13 μm, which enables all-day freshwater generation (Figure 4b). By applying the dual-mode film within a three-stage membrane distillation system, the testing result shows that 71.1% drinkable freshwater collection efficiency in the daytime and 0.1 L/m^2 day of dew water collection rate in the night can be achieved.

To explore the boundary conditions of dew-harvesting, Dong et al.[100] developed a theoretical model to explore the influence of various boundary conditions, including different emitters (blackbody and selective emitter), ambient temperature, relative humidity, and convection coefficient on mass flux, which can be solved by the following equations:

$$Q_{latent} = Q_{condenser}(T_{condenser}) - Q_{atm}(T_{ambient}, \mathrm{RH}) - (h + h_{parasitic})(T_{ambient} - T_{condenser}) \quad (10)$$

$$Q_{latent} = (Le)^n \frac{h}{\gamma}[\mathrm{RH} \times P_{H_2O}(T_{ambient}) - P_{H_2O}(T_{condenser})] \quad (11)$$

$$m = Q_{latent}/\Delta \quad (12)$$

where Q_{latent} is the latent heat released by the condensation process; $Q_{condenser}$ the thermal radiation of condenser; Q_{atm} the thermal radiation absorbed from the atmosphere; $T_{condenser}$ the temperature of the condenser; $T_{ambient}$ the temperature of ambient; RH the relative humidity; $h_{parasitic}$ all the parasitic heat transfer between the condenser and the ambient except for h, the convection that carries water vapor to the condenser; Le the Lewis number; n values for different scenarios; γ the psychrometer constant; P_{H_2O} the saturation vapor pressure; m the mass flux; and Δ the latent heat per unit mass. Solved using the above equation, Figure 4c clearly shows the result of mass flux under various boundary conditions. The performance of the selective emitter is better than that of the blackbody, particularly for high $T_{ambient}$ and low RH. For example, at $T_{ambient}$ = 20 °C with RH = 40%, the selective emitter achieves 13 g/m^2 hr of mass flux, and the blackbody fails in harvesting water under this condition. These theoretical analyses provide a clear guideline for the next material and device design.

> Designing materials and structures results in a significant increase in the three-level conversion efficiency. Nevertheless, there is still a long way to go for real applications in terms of performance, cost, and durability, especially for selective emitters.

With the development of the design and utilization of infrared light, profound progress has been made in direct solar desalination. This Focus Review systematically summarizes the background, the state-of-art progress, challenges, and opportunities of direct solar desalination by use of selective absorbers to obtain higher solar-to-vapor conversion efficiency, use of radiative energy to indirectly heat the water to resolve the salt-rejecting problem of the absorber, and use of radiative cooling to enhance the output of freshwater. Below, the authors share a few perspectives looking to the future:

Use of Selective Absorbers to Obtain Higher Solar-to-Vapor Conversion Efficiency. Although higher solar-to-vapor conversion efficiency has been achieved by lowering the vapor temperature,[20,22,101] here we focus on the production of high-temperature vapor/steam to enhance condensation, sterilization, and other applications. To achieve higher solar-to-vapor/steam conversion efficiency, higher-performance selective absorbers are highly desirable, especially for permeable selective absorbers. Interestingly, achieving selectivity with a porous structure can be inherently more difficult than with a planar structure. Pores act like light-trapping cavities that effectively increase the (apparent) emissivity. The apparent emissivity of a cavity can be approximated as $\varepsilon_{apparent} \approx \varepsilon/[\varepsilon + f(1 - \varepsilon)]$, where ε is the emissivity of the pore wall material and $f = A_{opening}/A_{wall}$ is the ratio of the pore opening area to the pore wall area. Because the value of f will be less than 1 for a pore, the result is that $\varepsilon_{apparent} > \varepsilon$. The overall result, which also holds for the effective absorptivity of the pore, is commonly known as the cavity effect. The above analysis is approximate because it does not assume the shape of the pore and further assumes diffusely reflecting pore walls and uniform irradiance inside the pore. Exact results for cavities of different geometries (cylindrical, conical, and spherical) are presented in ref 102. A simpler approximation $\varepsilon_{apparent} \approx \sqrt{\varepsilon}$, which holds near the opening of the pore, was presented by Buckley[103,104] and is useful as a rough estimate of the cavity effect. A surface with $\overline{\alpha}$ = 0.95 and $\overline{\varepsilon}$ = 0.05 achieves a selectivity of 19. Forming a pore out of this material yields $\overline{\alpha}_{apparent} \approx \sqrt{0.95}$ = 0.97 and

https://doi.org/10.1021/acsenergylett.1c00869
ACS Energy Lett. 2021, 6, 2645−2657

$\bar{\varepsilon}_{\text{apparent}} \approx \sqrt{0.05} = 0.22$, and the selectivity thus drops to 4.4. It is noteworthy that despite these inherent limitations, selectivity has been successfully implemented for various porous absorbers. It should be noted that the above analysis strictly holds only when the pore size is large compared to the wavelength, such that a geometrical optics treatment of the pore can be applied. For pores with dimensions on the order of the wavelength of light, a wave optics analysis should be applied. There may be interesting opportunities to augment the selectivity in a porous material with pore dimensions near the wavelength, if the cavity effect can be promoted for solar wavelengths and suppressed for infrared wavelengths.

Moreover, for permeable selective absorbers, the influence of water and vapor/steam on the absorber's thermal radiation still needs to be further explored. For example, when the material is hydrophilic, a large amount of water will appear on the absorber's surface. In this case, even if the material itself has a small emissivity, it may be challenging to achieve suppression of heat radiation because water is an excellent mid-infrared emitter. How to suppress the heat radiation generated by water from the perspective of material design requires further consideration. Also, compared with other desalination technologies such as reverse osmosis, portability is a crucial feature of direct solar desalination devices. The foldability of the absorber is essential to realize a portable device. However, to date, foldable selective absorbers are rarely reported.

Use of Radiative Energy to Indirectly Heat the Water to Resolve the Salt-Rejecting Problem of the Absorber. Through the analysis of the Focus Review, it can be seen that many salt-resistant technologies have been developed and achieved good results. As the only noncontact technology, it has significant advantages in durability and cycling. Meanwhile, it has to be mentioned that the current major limitation of this technology is its low efficiency. However, we think that there is still room for significant increase in the three-level conversion efficiency through the design of materials and structures (guidelines to increase the three-level efficiency (η_1, η_2, and η_3) can be found in eqs 6−8). Also, for radiative indirect heating, the absorber is often located above the bulk water, which mainly inhibits the escape of vapor/steam. Achieving effective escape of vapor/steam without losing the absorber's performance would also bring exciting opportunities.

Use of Radiative Cooling to Enhance the Output of Freshwater. The use of radiative cooling to increase water production is a very promising technology because it does not require additional energy input. For now, theories and models with different boundary conditions have made significant progress for the use of radiative cooling to increase water production. Nevertheless, for the design of materials and devices to be utilized for real applications, there is still a long way to go in terms of performance, cost, and durability, especially for selective emitters. Also, we can imagine that the ideal situation is to use radiative cooling to enhance condensation during the daytime and achieve dew-harvesting at night. Nevertheless, these are still in the early stages of research.

In sum, although some notable results have been achieved, there are still many areas in this field that require further research. We believe that, with more effort from researchers with a variety of backgrounds, more fundamental research and application breakthroughs are expected in the next few years.

AUTHOR INFORMATION

Corresponding Authors

Xiuqiang Li − *Thomas Lord Department of Mechanical Engineering and Materials Science, Duke University, Durham, North Carolina 27708, United States*; Email: xiuqiang.li@outlook.com

Po-Chun Hsu − *Thomas Lord Department of Mechanical Engineering and Materials Science, Duke University, Durham, North Carolina 27708, United States*; orcid.org/0000-0002-6509-9377; Email: pochun.hsu@duke.edu

Authors

Thomas Cooper − *Department of Mechanical Engineering, York University, Toronto, ON M3J 1P3, Canada*

Wanrong Xie − *Thomas Lord Department of Mechanical Engineering and Materials Science, Duke University, Durham, North Carolina 27708, United States*

Complete contact information is available at: https://pubs.acs.org/10.1021/acsenergylett.1c00869

Notes

The authors declare no competing financial interest.

Biographies

Xiuqiang Li obtained his Ph.D. at College of Engineering and Applied Sciences, Nanjing University. Currently, he is a postdoc at Duke University. His research focuses on water purification, personal heat management, and radiative cooling.

Thomas Cooper is an assistant professor at York University. He received his Ph.D. and MSc from ETH Zurich in 2014 and 2010, respectively, and his BASc from the University of Toronto in 2008, all in mechanical engineering. His research focuses on solar energy and converting it into useful forms.

Wanrong Xie is a graduate student in the Mechanical Engineering and Materials Science Department at Duke University. Her current research focuses on using conductive polymers for dynamic radiative heat modulation.

Po-Chun Hsu is an assistant professor at Duke University in the Thomas Lord Department of Mechanical Engineering and Materials Science. His lab focuses on light and heat management, nanophotonic materials, energy sustainability, and wearable technology. His radiative cooling textile was selected as a member of the "Ten World-Changing Ideas" by Scientific American. Group website: https://pochunhsu.group/.

ACKNOWLEDGMENTS

We thank Pratt School of Engineering at Duke University for the funding support.

REFERENCES

(1) https://ourworldindata.org/water-access (accessed 2021-02).

(2) Brown, A.; Matlock, M. White paper 2011, *106*, 19.

(3) Mekonnen, M.; Hoekstra, A. Four billion people facing severe water scarcity. *Science Advances* **2016**, *2*, e1500323.

(4) https://www.undp.org/content/undp/en/home/sustainable-development-goals/goal-6-clean-water-and-sanitation.html (accessed 2021-02).

(5) Pang, Y.; Zhang, J.; Ma, R.; Qu, Z.; Lee, E.; Luo, T. Solar−thermal water evaporation: a review. *ACS Energy Letters* **2020**, *5* (2), 437−456.

(6) Zhou, L.; Li, X.; Ni, G. W.; Zhu, S.; Zhu, J. The revival of thermal utilization from the Sun: interfacial solar vapor generation. *National Science Review* **2019**, *6* (3), 562−578.

(7) Ni, G.; Li, G.; Boriskina, S. V.; Li, H.; Yang, W.; Zhang, T.; Chen, G. Steam generation under one sun enabled by a floating structure with thermal concentration. *Nature Energy* **2016**, *1* (9), 16126.
(8) Chen, J.; Feng, J.; Li, Z.; Xu, P.; Wang, X.; Yin, W.; Wang, M.; Ge, X.; Yin, Y. Space-confined seeded growth of black silver nanostructures for solar steam generation. *Nano Lett.* **2019**, *19* (1), 400−407.
(9) Ghim, D.; Jiang, Q.; Cao, S.; Singamaneni, S.; Jun, Y.-S. Mechanically interlocked 1T/2H phases of MoS2 nanosheets for solar thermal water purification. *Nano Energy* **2018**, *53*, 949−957.
(10) Guan, Q. F.; Han, Z. M.; Ling, Z. C.; Yang, H. B.; Yu, S. H. Sustainable wood-based hierarchical solar steam generator: a biomimetic design with reduced vaporization enthalpy of water. *Nano Lett.* **2020**, *20* (8), 5699−5704.
(11) He, S.; Chen, C.; Kuang, Y.; Mi, R.; Liu, Y.; Pei, Y.; Kong, W.; Gan, W.; Xie, H.; Hitz, E.; Jia, C.; Chen, X.; Gong, A.; Liao, J.; Li, J.; Ren, Z. J.; Yang, B.; Das, S.; Hu, L. Nature-inspired salt resistant bimodal porous solar evaporator for efficient and stable water desalination. *Energy Environ. Sci.* **2019**, *12* (5), 1558−1567.
(12) Kim, J. U.; Kang, S. J.; Lee, S.; Ok, J.; Kim, Y.; Roh, S. H.; Hong, H.; Kim, J. K.; Chae, H.; Kwon, S. J.; Kim, T. i. Omnidirectional, broadband light absorption in a hierarchical nanoturf membrane for an advanced solar-vapor generator. *Adv. Funct. Mater.* **2020**, *30* (50), 2003862.
(13) Li, W.; Li, Z.; Bertelsmann, K.; Fan, D. E. Portable low-pressure solar steaming-collection unisystem with polypyrrole origamis. *Adv. Mater.* **2019**, *31* (29), 1900720.
(14) Li, X.; Min, X.; Li, J.; Xu, N.; Zhu, P.; Zhu, B.; Zhu, S.; Zhu, J. Storage and recycling of interfacial solar steam enthalpy. *Joule* **2018**, *2* (11), 2477−2484.
(15) Li, X.; Xu, W.; Tang, M.; Zhou, L.; Zhu, B.; Zhu, S.; Zhu, J. Graphene oxide-based efficient and scalable solar desalination under one sun with a confined 2D water path. *Proc. Natl. Acad. Sci. U. S. A.* **2016**, *113* (49), 13953−13958.
(16) Liang, H.; Liao, Q.; Chen, N.; Liang, Y.; Lv, G.; Zhang, P.; Lu, B.; Qu, L. Thermal efficiency of solar steam generation approaching 100% through capillary water transport. *Angew. Chem., Int. Ed.* **2019**, *58* (52), 19041−19046.
(17) Lu, Q.; Shi, W.; Yang, H.; Wang, X. Nanoconfined water-molecule channels for high-yield solar vapor generation under weaker sunlight. *Adv. Mater.* **2020**, *32* (42), 2001544.
(18) Meng, F. L.; Gao, M.; Ding, T.; Yilmaz, G.; Ong, W. L.; Ho, G. W. Modular deformable steam electricity cogeneration system with photothermal, water, and electrochemical tunable multilayers. *Adv. Funct. Mater.* **2020**, *30* (32), 2002867.
(19) Qi, D.; Liu, Y.; Liu, Y.; Liu, Z.; Luo, Y.; Xu, H.; Zhou, X.; Zhang, J.; Yang, H.; Wang, W.; Chen, X. Polymeric membranes with selective solution-diffusion for intercepting volatile organic compounds during solar-driven water remediation. *Adv. Mater.* **2020**, *32* (50), 2004401.
(20) Shi, Y.; Li, R.; Jin, Y.; Zhuo, S.; Shi, L.; Chang, J.; Hong, S.; Ng, K.-C.; Wang, P. A 3D photothermal structure toward improved energy efficiency in solar steam generation. *Joule* **2018**, *2* (6), 1171−1186.
(21) Singh, S. C.; ElKabbash, M.; Li, Z.; Li, X.; Regmi, B.; Madsen, M.; Jalil, S. A.; Zhan, Z.; Zhang, J.; Guo, C. Solar-trackable super-wicking black metal panel for photothermal water sanitation. *Nature Sustainability* **2020**, *3* (11), 938−946.
(22) Song, H.; Liu, Y.; Liu, Z.; Singer, M. H.; Li, C.; Cheney, A. R.; Ji, D.; Zhou, L.; Zhang, N.; Zeng, X.; Bei, Z.; Yu, Z.; Jiang, S.; Gan, Q. Cold vapor generation beyond the input solar energy limit. *Advanced Science* **2018**, *5* (8), 1800222.
(23) Tian, S.; Huang, Z.; Tan, J.; Cui, X.; Xiao, Y.; Wan, Y.; Li, X.; Zhao, Q.; Li, S.; Lee, C.-S. Manipulating interfacial charge-transfer absorption of cocrystal absorber for efficient solar seawater desalination and water purification. *ACS Energy Letters* **2020**, *5* (8), 2698−2705.
(24) Wang, W.; Shi, Y.; Zhang, C.; Hong, S.; Shi, L.; Chang, J.; Li, R.; Jin, Y.; Ong, C.; Zhuo, S.; Wang, P. Simultaneous production of fresh water and electricity via multistage solar photovoltaic membrane distillation. *Nat. Commun.* **2019**, *10* (1), 3012.
(25) Xu, Z.; Zhang, L.; Zhao, L.; Li, B.; Bhatia, B.; Wang, C.; Wilke, K. L.; Song, Y.; Labban, O.; Lienhard, J. H.; Wang, R.; Wang, E. N. Ultrahigh-efficiency desalination via a thermally-localized multistage solar still. *Energy Environ. Sci.* **2020**, *13* (3), 830−839.
(26) Zhao, F.; Zhou, X.; Shi, Y.; Qian, X.; Alexander, M.; Zhao, X.; Mendez, S.; Yang, R.; Qu, L.; Yu, G. Highly efficient solar vapour generation via hierarchically nanostructured gels. *Nat. Nanotechnol.* **2018**, *13* (6), 489−495.
(27) Zhou, X.; Zhao, F.; Guo, Y.; Rosenberger, B.; Yu, G. Architecting highly hydratable polymer networks to tune the water state for solar water purification. *Science Advances* **2019**, *5*, eaaw5484.
(28) Alvarez, P. J. J.; Chan, C. K.; Elimelech, M.; Halas, N. J.; Villagran, D. Emerging opportunities for nanotechnology to enhance water security. *Nat. Nanotechnol.* **2018**, *13* (8), 634−641.
(29) Chen, C.; Kuang, Y.; Hu, L. Challenges and opportunities for solar evaporation. *Joule* **2019**, *3* (3), 683−718.
(30) Irshad, M. S.; Arshad, N.; Wang, X. Nanoenabled photothermal materials for clean water production. *Global Challenges* **2021**, *5* (1), 2000055.
(31) Jun, Y. S.; Wu, X.; Ghim, D.; Jiang, Q.; Cao, S.; Singamaneni, S. Photothermal membrane water treatment for two worlds. *Acc. Chem. Res.* **2019**, *52* (5), 1215−1225.
(32) Kashyap, V.; Ghasemi, H. Solar heat localization: concept and emerging applications. *J. Mater. Chem. A* **2020**, *8* (15), 7035−7065.
(33) Li, X.; Ni, G.; Cooper, T.; Xu, N.; Li, J.; Zhou, L.; Hu, X.; Zhu, B.; Yao, P.; Zhu, J. Measuring conversion efficiency of solar vapor generation. *Joule* **2019**, *3* (8), 1798−1803.
(34) Tao, P.; Ni, G.; Song, C.; Shang, W.; Wu, J.; Zhu, J.; Chen, G.; Deng, T. Solar-driven interfacial evaporation. *Nature Energy* **2018**, *3* (12), 1031−1041.
(35) Wang, P. Emerging investigator series: the rise of nano-enabled photothermal materials for water evaporation and clean water production by sunlight. *Environ. Sci.: Nano* **2018**, *5* (5), 1078−1089.
(36) Zhang, P.; Liao, Q.; Yao, H.; Huang, Y.; Cheng, H.; Qu, L. Direct solar steam generation system for clean water production. *Energy Storage Materials* **2019**, *18*, 429−446.
(37) Zhao, F.; Guo, Y.; Zhou, X.; Shi, W.; Yu, G. Materials for solar-powered water evaporation. *Nature Reviews Materials* **2020**, *5* (5), 388−401.
(38) Zhou, J.; Gu, Y.; Liu, P.; Wang, P.; Miao, L.; Liu, J.; Wei, A.; Mu, X.; Li, J.; Zhu, J. Development and evolution of the system structure for highly efficient solar steam generation from zero to three dimensions. *Adv. Funct. Mater.* **2019**, *29* (50), 1903255.
(39) Zhu, L.; Gao, M.; Peh, C. K. N.; Ho, G. W. Recent progress in solar-driven interfacial water evaporation: Advanced designs and applications. *Nano Energy* **2019**, *57*, 507−518.
(40) Wang, Z.; Horseman, H.; Straub, A.; Yip, N.; Li, D.; Elimelech, M.; Lin, S. Pathways and challenges for efficient solar-thermal desalination. *Science Advances* **2019**, *5*, eaax0763.
(41) Cao, F.; McEnaney, K.; Chen, G.; Ren, Z. A review of cermet-based spectrally selective solar absorbers. *Energy Environ. Sci.* **2014**, *7* (5), 1615−1627.
(42) Li, Y.; Hao, J.; Song, H.; Zhang, F.; Bai, X.; Meng, X.; Zhang, H.; Wang, S.; Hu, Y.; Ye, J. Selective light absorber-assisted single nickel atom catalysts for ambient sunlight-driven CO_2 methanation. *Nat. Commun.* **2019**, *10* (1), 2359.
(43) Li, Y.; Lin, C.; Zhou, D.; An, Y.; Li, D.; Chi, C.; Huang, H.; Yang, S.; Tso, C. Y.; Chao, C. Y. H.; Huang, B. Scalable all-ceramic nanofilms as highly efficient and thermally stable selective solar absorbers. *Nano Energy* **2019**, *64*, 103947.
(44) Mandal, J.; Wang, D.; Overvig, A. C.; Shi, N. N.; Paley, D.; Zangiabadi, A.; Cheng, Q.; Barmak, K.; Yu, N.; Yang, Y. Scalable, ″dip-and-dry″ fabrication of a wide-angle plasmonic selective absorber for high-efficiency solar-thermal energy conversion. *Adv. Mater.* **2017**, *29* (41), 1702156.

https://doi.org/10.1021/acsenergylett.1c00869
ACS Energy Lett. 2021, 6, 2645−2657

(45) Dash, S.; de Ruiter, J.; Varanasi, K. Photothermal trap utilizing solar illumination for ice mitigation. *Science Advances* **2018**, *4*, eaat0127.

(46) Weinstein, L. A.; Loomis, J.; Bhatia, B.; Bierman, D. M.; Wang, E. N.; Chen, G. Concentrating solar power. *Chem. Rev.* **2015**, *115* (23), 12797−838.

(47) Xu, K.; Du, M.; Hao, L.; Mi, J.; Yu, Q.; Li, S. A review of high-temperature selective absorbing coatings for solar thermal applications. *Journal of Materiomics* **2020**, *6* (1), 167−182.

(48) Li, Y.; Lin, C.; Huang, J; Chi, C.; Huang, B. Spectrally selective absorbers/emitters for solar steam generation and radiative cooling-enabled atmospheric water harvesting. *Global Challenges* **2021**, *5* (1), 2000058.

(49) Huang, J.; He, Y.; Hu, Y.; Wang, X. Steam generation enabled by a high efficiency solar absorber with thermal concentration. *Energy* **2018**, *165*, 1282−1291.

(50) Wang, X.; Hsieh, M. L.; Bur, J. A.; Lin, S. Y.; Narayanan, S. Capillary-driven solar-thermal water desalination using a porous selective absorber. *Materials Today Energy* **2020**, *17*, 100453.

(51) Lin, K. T.; Lin, H.; Yang, T.; Jia, B. Structured graphene metamaterial selective absorbers for high efficiency and omnidirectional solar thermal energy conversion. *Nat. Commun.* **2020**, *11* (1), 1389.

(52) Zhang, C.; Shi, Y.; Shi, L.; Li, H.; Li, R.; Hong, S.; Zhuo, S.; Zhang, T.; Wang, P. Designing a next generation solar crystallizer for real seawater brine treatment with zero liquid discharge. *Nat. Commun.* **2021**, *12* (1), 998.

(53) Zhou, L.; Zhuang, S.; He, C.; Tan, Y.; Wang, Z.; Zhu, J. Self-assembled spectrum selective plasmonic absorbers with tunable bandwidth for solar energy conversion. *Nano Energy* **2017**, *32*, 195−200.

(54) Chang, C.; Tao, P.; Xu, J.; Fu, B.; Song, C.; Wu, J.; Shang, W.; Deng, T. High-efficiency superheated steam generation for portable sterilization under ambient pressure and low solar flux. *ACS Appl. Mater. Interfaces* **2019**, *11* (20), 18466−18474.

(55) Chang, C.; Tao, P.; Fu, B.; Xu, J.; Song, C.; Wu, J.; Shang, W.; Deng, T. Three-dimensional porous solar-driven interfacial evaporator for high-efficiency steam generation under low solar flux. *ACS Omega* **2019**, *4* (2), 3546−3555.

(56) Xue, G.; Chen, Q.; Lin, S.; Duan, J.; Yang, P.; Liu, K.; Li, J.; Zhou, J. Highly efficient water harvesting with optimized solar thermal membrane distillation device. *Global Challenges* **2018**, *2* (5−6), 1800001.

(57) Chiavazzo, E.; Morciano, M.; Viglino, F.; Fasano, M.; Asinari, P. Passive solar high-yield seawater desalination by modular and low-cost distillation. *Nature Sustainability* **2018**, *1* (12), 763−772.

(58) Zhao, L.; Bhatia, B.; Zhang, L.; Strobach, E.; Leroy, A.; Yadav, M. K.; Yang, S.; Cooper, T. A.; Weinstein, L. A.; Modi, A.; Kedare, S. B.; Chen, G.; Wang, E. N. A passive high-temperature high-pressure solar steam generator for medical sterilization. *Joule* **2020**, *4* (12), 2733−2745.

(59) Li, H.; Yan, Z.; Li, Y.; Hong, W. Latest development in salt removal from solar-driven interfacial saline water evaporators: Advanced strategies and challenges. *Water Res.* **2020**, *177*, 115770.

(60) Zhang, Y.; Xiong, T.; Nandakumar, D. K.; Tan, S. C. Structure architecting for salt-rejecting solar interfacial desalination to achieve high-performance evaporation with in situ energy generation. *Advanced Science* **2020**, *7* (9), 1903478.

(61) Xu, W.; Hu, X.; Zhuang, S.; Wang, Y.; Li, X.; Zhou, L.; Zhu, S.; Zhu, J. Flexible and salt resistant janus absorbers by electrospinning for stable and efficient solar desalination. *Advanced Energy Materials* **2018**, *8* (14), 1702884.

(62) Kuang, Y.; Chen, C.; He, S.; Hitz, E. M.; Wang, Y.; Gan, W.; Mi, R.; Hu, L. A high-performance self-regenerating solar evaporator for continuous water desalination. *Adv. Mater.* **2019**, *31* (23), 1900498.

(63) Ni, G.; Zandavi, S. H.; Javid, S. M.; Boriskina, S. V.; Cooper, T. A.; Chen, G. A salt-rejecting floating solar still for low-cost desalination. *Energy Environ. Sci.* **2018**, *11* (6), 1510−1519.

(64) Fang, Q.; Li, T.; Lin, H.; Jiang, R.; Liu, F. Highly efficient solar steam generation from activated carbon fiber cloth with matching water supply and durable fouling resistance. *ACS Applied Energy Materials* **2019**, *2* (6), 4354−4361.

(65) Zhang, Q.; Yang, H.; Xiao, X.; Wang, H.; Yan, L.; Shi, Z.; Chen, Y.; Xu, W.; Wang, X. A new self-desalting solar evaporation system based on a vertically oriented porous polyacrylonitrile foam. *J. Mater. Chem. A* **2019**, *7* (24), 14620−14628.

(66) Hu, R.; Zhang, J.; Kuang, Y.; Wang, K.; Cai, X.; Fang, Z.; Huang, W.; Chen, G.; Wang, Z. A Janus evaporator with low tortuosity for long-term solar desalination. *J. Mater. Chem. A* **2019**, *7* (25), 15333−15340.

(67) Zhang, Y.; Xiong, T.; Suresh, L.; Qu, H.; Zhang, X.; Zhang, Q.; Yang, J.; Tan, S. Guaranteeing complete salt rejection by channeling saline water through fluidic photothermal structure toward synergistic zero energy clean water production and in situ energy generation. *ACS Energy Letters* **2020**, *5*, 3397−3404.

(68) Zhang, Y.; Zhang, H.; Xiong, T.; Qu, H.; Koh, J. J.; Nandakumar, D.; Wang, J.; Tan, S. Manipulating unidirectional fluid transportation to drive sustainable solar water extraction and brine-drenching induced energy generation. *Energy Environ. Sci.* **2020**, *13* (12), 4891−4902.

(69) Xu, N.; Li, J.; Wang, Y.; Fang, C.; Li, X.; Wang, Y.; Zhou, L.; Zhu, B.; Wu, Z.; Zhu, S.; Zhu, J. A water lily−inspired hierarchical design for stable and efficient solar evaporation of high-salinity brine. *Science Advances* **2019**, *5*, eaaw7013.

(70) Chen, J.; Yin, J. L.; Li, B.; Ye, Z.; Liu, D.; Ding, D.; Qian, F.; Myung, N. V.; Zhang, Q.; Yin, Y. Janus evaporators with self-recovering hydrophobicity for salt-rejecting interfacial solar desalination. *ACS Nano* **2020**, *14* (12), 17419−17427.

(71) Yang, Y.; Zhao, H.; Yin, Z.; Zhao, J.; Yin, X.; Li, N.; Yin, D.; Li, Y.; Lei, B.; Du, Y.; Que, W. A general salt-resistant hydrophilic/hydrophobic nanoporous double layer design for efficient and stable solar water evaporation distillation. *Mater. Horiz.* **2018**, *5* (6), 1143−1150.

(72) Liu, Z.; Wu, B.; Zhu, B.; Chen, Z.; Zhu, M.; Liu, X. Continuously producing watersteam and concentrated brine from seawater by hanging photothermal fabrics under sunlight. *Adv. Funct. Mater.* **2019**, *29* (43), 1905485.

(73) Shi, Y.; Zhang, C.; Li, R.; Zhuo, S.; Jin, Y.; Shi, L.; Hong, S.; Chang, J.; Ong, C.; Wang, P. Solar evaporator with controlled salt precipitation for zero liquid discharge desalination. *Environ. Sci. Technol.* **2018**, *52* (20), 11822−11830.

(74) Wu, L.; Dong, Z.; Cai, Z.; Ganapathy, T.; Fang, N. X.; Li, C.; Yu, C.; Zhang, Y.; Song, Y. Highly efficient three-dimensional solar evaporator for high salinity desalination by localized crystallization. *Nat. Commun.* **2020**, *11* (1), 521.

(75) Xia, Y.; Hou, Q.; Jubaer, H.; Li, Y.; Kang, Y.; Yuan, S.; Liu, H.; Woo, M. W.; Zhang, L.; Gao, L.; Wang, H.; Zhang, X. Spatially isolating salt crystallisation from water evaporation for continuous solar steam generation and salt harvesting. *Energy Environ. Sci.* **2019**, *12* (6), 1840−1847.

(76) Zhuang, P.; Fu, H.; Xu, N.; Li, B.; Xu, J.; Zhou, L. Free-standing reduced graphene oxide (rGO) membrane for salt-rejecting solar desalination via size effect. *Nanophotonics* **2020**, *9* (15), 4601−4608.

(77) Zeng, J.; Wang, Q.; Shi, Y.; Liu, P.; Chen, R. Osmotic pumping and salt rejection by polyelectrolyte hydrogel for continuous solar desalination. *Adv. Energy Mater.* **2019**, *9* (38), 1900552.

(78) Cooper, T. A.; Zandavi, S. H.; Ni, G. W.; Tsurimaki, Y.; Huang, Y.; Boriskina, S. V.; Chen, G. Contactless steam generation and superheating under one sun illumination. *Nat. Commun.* **2018**, *9* (1), 5086.

(79) Menon, A. K.; Haechler, I.; Kaur, S.; Lubner, S.; Prasher, R. S. Enhanced solar evaporation using a photo-thermal umbrella for wastewater management. *Nature Sustainability* **2020**, *3* (2), 144−151.

(80) Bian, Y.; Tian, Y.; Tang, K.; Li, W.; Zhao, L.; Yang, Y.; Ye, J.; Gu, S. Sustainable solar evaporation from solute surface via energy downconversion. *Global Challenges* **2021**, *5* (1), 2000077.

(81) Gupta, B.; Mandraha, T.; Edla, P.; Pandya, M. Thermal modeling and efficiency of solar water distillation: a review. *American Journal of Engineering Research (AJER)* **2013**, *2*, 203−213.
(82) El-Sebaii, A. A. On effect of wind speed on passive solar still performance based on inner/outer surface temperatures of the glass cover. *Energy* **2011**, *36* (8), 4943−4949.
(83) Vinoth Kumar, K.; Kasturi Bai, R. Performance study on solar still with enhanced condensation. *Desalination* **2008**, *230* (1−3), 51−61.
(84) Muselli, M.; Beysens, D.; Marcillat, J.; Milimouk, I.; Nilsson, T.; Louche, A. Dew water collector for potable water in Ajaccio. *Atmos. Res.* **2002**, *64*, 297−312.
(85) Maestre-Valero, J. F.; Martínez-Alvarez, V.; Baille, A.; Martín-Górriz, B.; Gallego-Elvira, B. Comparative analysis of two polyethylene foil materials for dew harvesting in a semi-arid climate. *J. Hydrol.* **2011**, *410* (1−2), 84−91.
(86) Raman, A. P.; Anoma, M. A.; Zhu, L.; Rephaeli, E.; Fan, S. Passive radiative cooling below ambient air temperature under direct sunlight. *Nature* **2014**, *515* (7528), 540−544.
(87) Chen, Z.; Zhu, L.; Li, W.; Fan, S. Simultaneously and synergistically harvest energy from the sun and outer space. *Joule* **2019**, *3* (1), 101−110.
(88) Chen, Z.; Zhu, L.; Raman, A.; Fan, S. Radiative cooling to deep sub-freezing temperatures through a 24-h day-night cycle. *Nat. Commun.* **2016**, *7*, 13729.
(89) Kim, H.; Rao, S. R.; Kapustin, E. A.; Zhao, L.; Yang, S.; Yaghi, O. M.; Wang, E. N. Adsorption-based atmospheric water harvesting device for arid climates. *Nat. Commun.* **2018**, *9* (1), 1191.
(90) Li, X.; Sun, B.; Sui, C.; Nandi, A.; Fang, H.; Peng, Y.; Tan, G.; Hsu, P. C. Integration of daytime radiative cooling and solar heating for year-round energy saving in buildings. *Nat. Commun.* **2020**, *11* (1), 6101.
(91) Li, X.; Xie, W.; Sui, C.; Hsu, P.-C. Multispectral thermal management designs for net-zero energy buildings. *ACS Materials Letters* **2020**, *2* (12), 1624−1643.
(92) Zhou, L.; Song, H.; Liang, J.; Singer, M.; Zhou, M.; Stegenburgs, E.; Zhang, N.; Xu, C.; Ng, T.; Yu, Z.; Ooi, B.; Gan, Q. A polydimethylsiloxane-coated metal structure for all-day radiative cooling. *Nature Sustainability* **2019**, *2* (8), 718−724.
(93) Zhai, Y.; Ma, Y.; David, S. N.; Zhao, D.; Lou, R.; Tan, G.; Yang, R.; Yin, X. Scalable-manufactured randomized glass-polymer hybrid metamaterial for daytime radiative cooling. *Science* **2017**, *355*, 1062−1066.
(94) Mandal, J.; Fu, Y.; Overvig, A. C.; Jia, M.; Sun, K.; Shi, N. N.; Zhou, H.; Xiao, X.; Yu, N.; Yang, Y. Hierarchically porous polymer coatings for highly efficient passive daytime radiative cooling. *Science* **2018**, *362*, 315−319.
(95) Li, T.; Zhai, Y.; He, S.; Gan, W.; Wei, Z.; Heidarinejad, M.; Dalgo, D.; Mi, R.; Zhao, X.; Song, J.; Dai, J.; Chen, C.; Aili, A.; Vellore, A.; Martini, A.; Yang, R.; Srebric, J.; Yin, X.; Hu, L. A radiative cooling structural material. *Science* **2019**, *364*, 760−763.
(96) Leroy, A.; Bhatia, B.; Kelsall, C. C.; Castillejo-Cuberos, A.; Di Capua, H. M.; Zhao, L.; Zhang, L.; Guzman, A. M.; Wang, E. N. High-performance subambient radiative cooling enabled by optically selective and thermally insulating polyethylene aerogel. *Science Advances* **2019**, *5*, eaat9480.
(97) Zhou, M.; Song, H.; Xu, X.; Shahsafi, A.; Xia, Z.; Ma, Z.; Kats, M. A.; Zhu, J.; Ooi, B. S.; Gan, Q.; Yu, Z. Vapor condensation with daytime radiative cooling. *Proc. Natl. Acad. Sci. U. S. A.* **2021**, *118* (14), e2019292118.
(98) Eriksson, T.; Granqvist, C. Radiative cooling computed for model atmospheres. *Appl. Opt.* **1982**, *21*, 4381−4388.
(99) Xu, J.; Zhang, J.; Fu, B.; Song, C.; Shang, W.; Tao, P.; Deng, T. All-day freshwater harvesting through combined solar-driven interfacial desalination and passive radiative cooling. *ACS Appl. Mater. Interfaces* **2020**, *12* (42), 47612−47622.
(100) Dong, M.; Zhang, Z.; Shi, Y.; Zhao, X.; Fan, S.; Chen, Z. Fundamental limits of the dew-harvesting technology. *Nanoscale Microscale Thermophys. Eng.* **2020**, *24* (1), 43−52.
(101) Li, X.; Li, J.; Lu, J.; Xu, N.; Chen, C.; Min, X.; Zhu, B.; Li, H.; Zhou, L.; Zhu, S.; Zhang, T.; Zhu, J. Enhancement of interfacial solar vapor generation by environmental energy. *Joule* **2018**, *2* (7), 1331−1338.
(102) Sparrow, E. M.; Cess, R. D. *Radiation Heat Transfer, Augmented Edition*; 1976
(103) Buckley, H. On the radiation from the inside of a circular cylinder: Part I. *Philos. Mag.* **1927**, *4*, 753−762.
(104) Buckley, H. On the radiation from the inside of a circular cylinder: Part II. *Philos. Mag.* **1928**, *6*, 447−457.

https://doi.org/10.1021/acsenergylett.1c00869
ACS Energy Lett. 2021, 6, 2645−2657